Available online at www.sciencedirect.com

ScienceDirect

IFAC Papers Online CONFERENCE PAPER ARCHIVE

IFAC PapersOnLine 55-27 (2022) 7–12

Omnidirectional All-Terrain Screw-Driven Robot Design, Modeling, and Application in Humanitarian Demining ⋆

Opeyemi Oladunjoye * Christina Maffattone * Julia Al-Nawal * Sofia Fasullo ** Eva Greenspan ** Jeffrey Koller * Alex Nikulin ** Timothy de Smet * Garrett M. Clayton ***

* *Department of Mechanical Engineering, Villanova University, Villanova, PA, 19085, USA (e-mail: garrett.clayton@villanova.edu).*
** *Department of Geology, Binghamton University, Binghamton, NY, 13902, USA (e-mail: anikulin@binghamton.edu)*
*** *Department of Anthropology, Binghamton University, Binghamton, NY, 13902, USA (e-mail: tdesmet@binghamton.edu)*

Abstract: In this paper, we present a screw-propelled omnidirectional mobile robot with the ability to navigate on a variety of terrains. The robot design, kinematic and inverse-kinematic models, and testing on different terrains are presented. In the end it was determined that the robot could operate on most terrains in any direction. To show the potential for the robot in field applications, the robot was used in a simulated humanitarian demining scenario. The robot coupled with a mine detection sensor showed promise for this use.

Keywords: Omnidirectional, Humanitarian Demining, Mobile Robot, MFAM, All-Terrain, Screw-Bot, Cambodia.

1. INTRODUCTION

In this paper, we present a low-cost screw-propelled mobile robot prototype with the ability to navigate rough terrain. The robot's design, kinematic and inverse-kinematic models, and testing on different terrains are discussed. Results from the application of the robot to humanitarian demining show the potential of the robot for field use.

One of the first screw-propelled vehicles was created by James and Ira Peavey for carrying and delivering wood in mountainous terrain (He and Long (2018)). In the 1920's, The Armstead Snow Motor and Fordson Snowmobile utilized a screw-drive for operation on snow. Screw driven vehicles used during World War II include the Marsh Screw Amphibian (MSA) (Neumeyer and Jones (1965)) and ZIL (He and Long (2018)), which were studied and developed further in the 1960s and 1970s. All these applications used a double screw design, where a pair of parallel cylinders with opposite handedness (i.e., the direction of the thread), can perform non-holonomic motion (He and Long (2018)). In contrast to these vehicles, we choose an inline screw design where two sets of inline cylinders are put in parallel, see Fig. 1. This design is advantageous because it allows omnidirectional motion with the potential more power (Freeberg (2010)).

Small screw-driven robots can be found in recent literature that utilize a double screw implementation (He and Long (2018); Osiński and Szykiedans (2015)). Our robot differs from these examples due to its inline screws and rugged design. Existing models of screw robots and corresponding control implementation such as Nagaoka et al. (2009) and He and Long (2018) were utilized in this work. Studies of omnidirectional robots, e.g. using mecanum wheels, also provide insight on the kinematic modelling of the presented robot (Taheri et al. (2015)).

In this paper, we designed and built an omnidirectional in-line screw-propelled robot. The kinematic and inverse kinematic configuration of the robot were determined allowing us to design trajectories. Terrain tests revealed that the robot can traverse sideways and rotate about its center on all terrains with some limitation on forward/backward movement on some terrains. Following the initial field

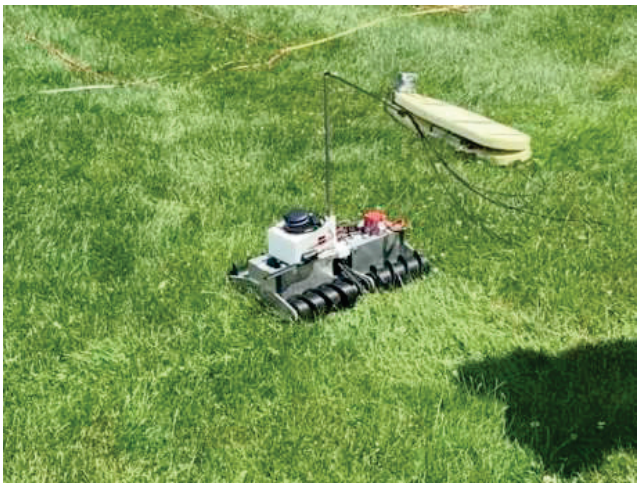

Fig. 1. Screw-Bot and MFAM testing Setup

⋆ The research was supported in part by the United States National Science Foundation (NSF) through grant OISE-1658696.

10.1016/j.ifacol.2022.10.480

tests, the robot was equipped with a miniature fabricated atomic magnetometer (MFAM) – also shown in Fig. 1 behind the robot – and used to find buried landmines in a simulated minefield. Our prototype and testing show the potential for the robot to be used in the field.

The remainder of this paper is structured as follows: Sec. 2 discusses background and context, Sec. 3 is about design of the robot, Sec. 4 presents the robot kinematics, Sec. 5 deals with terrain testing and Sec. 6 deals with the MFAM testing followed by conclusion.

2. BACKGROUND AND CONTEXT

One of the driving forces behind the development of this robot is its potential use in demining efforts in Southeast Asia, specifically Cambodia. Three decades of conflict in Cambodia has led to mass contamination with unexploded ordnance (UXO) – military ammunition/bombs i.e landmines, cluster munitions, IEDs etc. From 1965 to 1973, the United States dropped more than 2.8 tons of ordnance on land surfaces (Chan (2013)). Many landmines were buried after the Vietnamese ousted the Khmer Rouge. After the Vietnamese left in 1979, guerilla groups continued to use landmines for defensive purposes as unrest remained in the country (Chan (2013)). These events led to the contamination of 46.1% of villages and 4,544 km^2 of land, putting 45.2% of Cambodians at risk (Chan (2013)). Unfortunately, UXO continue to maim or kill Cambodians to this day – 64,843 from 1979 to 2019 (OpenDevelopment Cambodia (2020)). Furthermore, UXO contamination threatens the livelihood and activities of communities. Poor Cambodians face the dilemma between starvation or mine-related death and have restricted access to neighboring villages, markets, health centers and schools (OpenDevelopment Cambodia (2020)).

Before 1993, demining in Cambodia had little technological support; Villagers would remove landmines to clear land for personal use (DeAngelo (2018)). Since then, demining has become more standardized and has begun to use more technology. Demining typically consists of four stages: Identifying suspected minefields, brush clearance, mine detection and then mine detonation or disarming. The mine detection process uses a broad range of sensors, including electromagnetic induction (EMI) and ground penetrating radar (GPR). Other methods inculde the use of African pouched rats (DeAngelo (2018)) and dogs. There has been significant interest in the use of robots in demining, for example gryphon, a humanitarian deming robot (Fukushima et al. (2008)), but broad adoption has not come easy. The work presented in this paper follows work in EOD (Fracchia et al. (2015)) for use in low-income countries and tackles a major challenge to humanitarian demining robots – tough terrain and dense vegetation. Currently, brush clearance of suspected minefields takes a great deal of time and resources. Thus, we developed a robot capable of aiding humanitarian demining efforts in Cambodia before brush is cleared.

3. DESIGN

In order to address the problem of operation in rough terrain with heavy vegetation, Wheels, tank treads, and screws were considered for the robot. The following design considerations were explored:

Maneuverability Wheels and tank treads do not provide omnidirectional motion, with tank treads offering better operation on a broader range of terrains. Screws have the potential to provide omnidirectional motion and are good for natural terrain types (sand, gravel, etc.). Maneuverability to avoid obstacles such as large rocks, holes in the ground, debris, and foliage is especially important.

Maintenance and Complexity A wheeled drive mechanism is perhaps the easiest to maintain and are the easiest to assemble. Tank treads tend to be more complicated and require more maintenance. Screws were determined to be in between these two options with regard to complexity and maintenance.

Cost and Availability Wheels are perhaps the cheapest and most easy to procure. Tanks treads are more expensive and less available. Screw drives are not necessarily available so it is difficult to determine cost. They can, however be 3D printed so cost is dependent on material.

After considering these designs and their characteristics, the wheels and screws ranked closely. Ultimately, the screw design was chosen because of its omnidirectional nature and potential on varying terrains. Multiple screw configurations were considered, including the double screw and in-line screw designs discussed previously, as well as cross-screw and diamond-screw designs (Freeberg (2010)). In the end the double screw and in-line screw design were focused on. Compared to the in-line screw design, the double screw is not fully omnidirectional, the locomotive capabilities vary depending on terrain, and the turning radius is terrain dependent (Freeberg (2010)). The in-line screw is omnidirectional on a multitude of terrains, rotates about its center, and the alignment of the screws result in more precise movement.

In the end an in-line screw design was chosen, as seen in Fig. 2. Screws were 3D printed out of ABS plastic and Onyx—a composite material made from nylon and

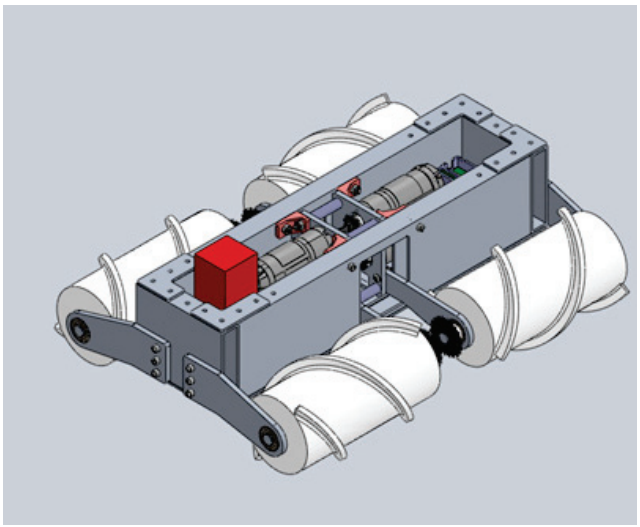

Fig. 2. Computer Aided Design (CAD) model of screw-bot assembly

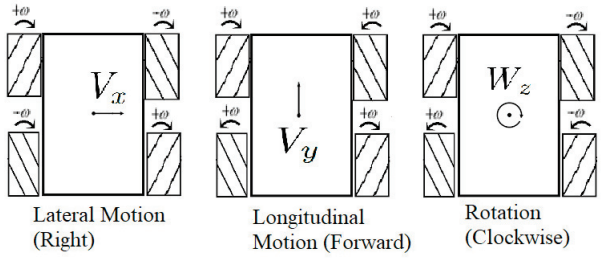

Fig. 3. Robot's Degrees of Freedom

carbon fiber. Aluminum 6061 was chosen as the material for all structural components since it provides sufficient strength for the application, is a fairly light metal, and is non-ferrous (advantages to limit sensor noise.) The main frame is held together with rivets and the screw arms are attached with nuts and bolts. There are four motors contained in the main body of the chassis. Each motor has a planetary gearbox attached to it which then transfers its rotation via a chain to the screws. The robot was also covered with a mu-metal mesh to avoid electromagnetic contamination to limit interference with potential sensors.

4. ROBOT KINEMATICS

The interaction of the two clockwise and two anticlockwise screws makes the kinematics of the robot a topic of interest. The relationship between angular velocities of the screws and omnidirectional behavior was analyzed, modeled, and simulated to serve as a basis for control of the robot.

4.1 Coordinate Systems

Figure 3 presents a model of how screw angular velocities are related to its 3 degrees of freedom —- lateral (sideways) translation, longitudinal (forward/backward) translation, and rotation about its center (Safar et al. (2018)). These can be represented with velocity vector

$$V_r = [V_x \; V_y \; W_z]^\top, \tag{1}$$

where V_x and V_y represent the velocities in lateral x and longitudianl y directions, respectively, and W_z is rotation about the center axis z.

Rotation of a screw is assumed to trigger two simultaneous forces – a lateral force in the direction it rotates and a longitudinal force. This longitudinal force is forward when a screw rotates in the same direction as its handedness and backward when it rotates opposite to its handedness. Since there are four screws, the summation of these forces allows the robot to move in any direction, rotate about its center of gravity, or do both simultaneously.

Figure 4 shows a basic robot coordinate system to provide a basis for mathematical modelling its kinematics. The center of gravity (COG) of the robot is the point of interest to represent the robot's position. In addition to a global fixed frame $(X - Y)$, a body frame is attached $(X' - Y')$ to the robot's COG because the robot's three degrees of freedom are relative to the body frame. The body frame's x-axis represents lateral translation, y-axis

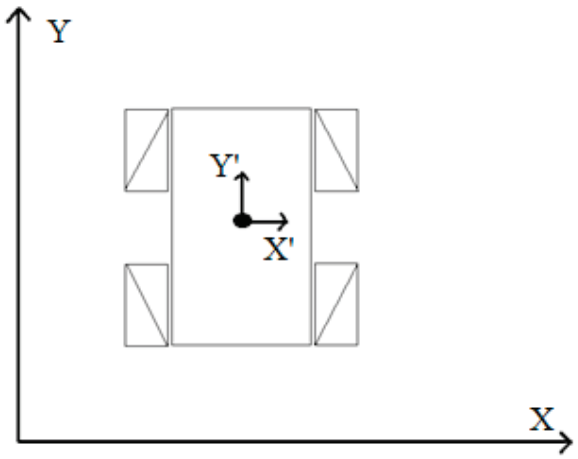

Fig. 4. Coordinate Frames

represents longitudinal translation and the robot rotates about its z-axis.

4.2 Inverse and Forward Kinematics

The local body frame kinematic equations were derived by modifying and combining screw modelling techniques from Safar et al. (2018) and Taheri et al. (2015). For our derivation, subscripts 1,2,3 and 4 were used to represent top left, top right, bottom left and bottom right screws, respectively. The first relationship that was derived was the inverse kinematic equation 2

$$w = M \times V_r. \tag{2}$$

Where ω is the angular velocity vector of the four screws, in $\mathrm{rad\,s^{-1}}$, defined as $\omega = [\omega_1 \; \omega_2 \; \omega_3 \; \omega_4]^T$, and V_r is the velocity vector from (1). M is the inverse Jacobian, J^{-1}, a 4×3 matrix with the following rows

$$M(i, 1:3) = \left[\frac{\sin(\gamma_i)}{r_i \cos(\gamma_i)} \;\; \frac{1}{r_i} \;\; \frac{L\cos(\gamma_i)}{r_i} - \frac{\sin(\alpha_i)\sin(\gamma_i)}{r_i \cos(\gamma_i)}\right]$$

Where γ_i is the helix angle (positive for right handed screws, negative for left handed screws), r_i is the radius of the screw, L is the length of a line drawn connecting the robot center to the screw center, α_i is the four quadrant angle formed by L for each screw and $i = 1, 2, 3, 4$. The forward kinematic equation is

$$V_r = N \times w \tag{3}$$

Where N is the pseudo-inverse of the inverse Jacobian M, obtained by the equation

$$N = (M^\top \times M)^{-1} \times M^\top \tag{4}$$

4.3 Experimental Validation

In order to verify the kinematic model presented above, the inverse kinematic model was used to determine the screw angular velocities that would result in the robot rotating clockwise while following a semi-circular path over a time of 20π seconds, shown as a solid line in Fig. 5. The position and orientation of the robot were defined as

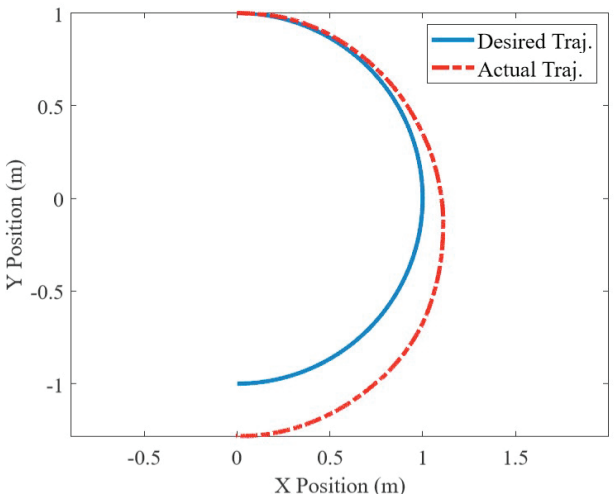

Fig. 5. Desired Versus Actual Robot Trajectory

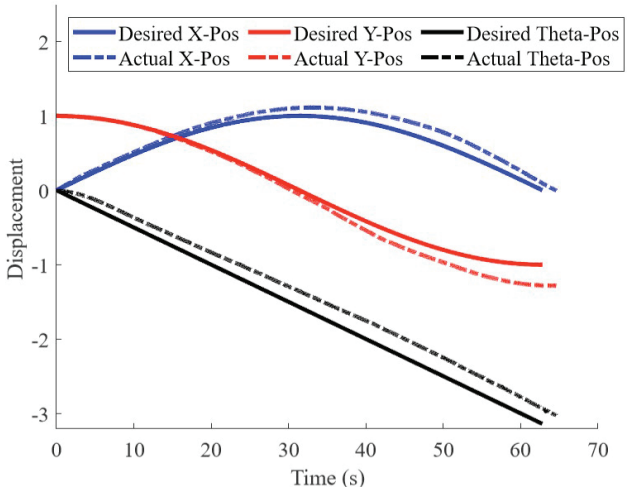

Fig. 6. Comparison of Position/Orientation with Time

$$[x(t)\ y(t)\ \theta(t)] = \left[\sin(\tfrac{t}{10})\ \cos(\tfrac{t}{10})\ \tfrac{-t}{10}\right]. \qquad (5)$$

The trajectories are shown as solid lines in Fig. 6. The inverse kinematic equation in (2) was used to determine that a constant set of angular velocities, $\omega = [1.8522\ -1.8887\ -1.0638\ 1.0273]^T \,\mathrm{rad\,s^{-1}}$ was needed to follow the desired trajectory. To verify our kinematic relationships, the screws were commanded to rotate at the calculated input angular velocities and the resulting motion was captured with a VICON motion capture system.

As Fig. 5 and Fig. 6 show, the robot imitated the semi-circular path and simultaneous clockwise rotation described by (5) with reasonable accuracy. It is noted that the positions and orientation diverged from desired, with increasing tracking error as time progressed. These discrepancies can be explained from uncertainties in measured parameters, delays in data transfer, unmodelled friction. Even with these errors, the results show that the kinematic models in (2) and (3) represent the behaviour of the robot, with some room for improvement. Moving forward, our understanding of robot kinematics will allow us to perform correct angular velocities input combinations to obtain all types of requisite robot motion. Furthermore, this creates an opportunity to explore feedback control of the robot in future work.

5. TERRAIN TESTING

Terrain testing of the robot was carried out to assess its ability to function on different terrains. Testing was done with a set of Polylactic acid (PLA) screws (Fig. 8), and a set of smaller screws (diameter reduced from 3.6 to 2.7 inch and pitch reduced from 6.25 to 4.17) made with Onyx, see Fig. 7 in order to see how different screw material and design might change the results.

With these two sets of screws, the three types of motions were tested in the following terrains: Grass (Flat, Sloped, Turfed and heavy brush), Sand, Wood chips and Concrete Tiles. In these experiments, the robot was operated under remote control. A 10 foot mobility test was performed by laying a measuring tape on the ground and attempting to perform straight line translation for the whole 10 feet and back. The robot was also rotated 360° on the terrain to assess its rotational capabilities. Figures 7 and 8 show examples of tests performed with Onyx and PLA screws, respectively.

The performance on these terrains was assessed qualitatively using a terrain performance scale adapted from Freeberg (2010), A grade from 0-3 was used as follows:

- **0:** Does not move
- **1:** Moves briefly with frequent stops and path deviations
- **2:** Moves fairly well with occasional stops and path deviations
- **3:** Moves consistently well with no stops or path deviations

Table 1: Terrain Performance Matrix

Terrain	PLA Screws			Onyx Screws		
	Long.	Lat.	Rot.	Long.	Lat.	Rot.
Grass, Flat	3	3	3	3	3	3
Grass, Slope	3	3	3	3	3	3
Grass, Turf	3	3	3	3	3	3
Grass, Brush	2	3	3	3	3	3
Sand, Soft	1	3	3	1	2	3
Woodchips	2	3	3	2	3	3
Tile, Brick	0	3	3	0	3	3

As shown in Table 1, sideways and rotational locomotion worked well in most terrains. Forward/backward motion,

Fig. 7. Longitudinal motion on Wood chips with Onyx

Fig. 8. Lateral Motion on Grass Slope with PLA screws

however, was achieved in grass but struggled for other terrain. The following specific notes were made

(1) Onyx Screws performed slightly better in brush due to their compact design and material properties
(2) Longitudinal motion was impossible on Concrete tiles as the screws need to dig into the terrain to move forward.
(3) Longitudinal motion was very difficult in the soft sand. This can be attributed to the lack of ground clearance, which led to sand choking the drive system whenever the screws dug into the sand.
(4) The robot's ability to rotate and move laterally could make up for issues in forward/backward motion.

6. APPLICATION: DEMINING

Magnetic surveying focuses on identification of anthropogenic or geological anomalies standing out from the background magnetic field of the Earth. Modern laser-pumped magnetometers rely on optical pumping of cesium atoms to record the procession of atomic spins, which are sensitive to picoTesla-scale magnetic variations. This heightened sensitivity and reduced magnetometer mass and dimensions allows their use in near-surface humanitarian geophysics surveys targeting detection of ferrous metal-containing landmines, UXOs, and IEDs.

In our experiments we deployed a reliable Microfabricated Atomic Magnetometer (MFAM) by Geometrics, an instrument that is less than 100 x 20 x 10cm in dimension in its casing and that has previously demonstrated promising results in detection of large UXOs and orphaned and abandoned oil and gas wells with similar geophysical signatures in aerial drone-based surveys (Nikulin and de Smet (2019);Nikulin et al. (2020);de Smet et al. (2021)). The small mass and relatively small dimensions of the MFAM allowed an easy pairing with the ground-based screw-bot developed in this work. Apart from the sensor package, the MFAM is equipped with a recording unit, GPS and timing system, allowing both spatial and temporal positioning of acquired data sets. A vertical metal arm was connected to the main body of the robot with a 3D printed mount, and a ball joint was attached at the top to another metal arm and rope attached to the MFAM sensor. This way, the robot could rotate without tangling the ropes connected to the sensor, which were kept away from the screws.

Prior to integration of the MFAM and the Screw Bot, multiple stand-alone sensor field tests were conducted by

(a) Control test

(b) Robot test

Fig. 9. MFAM tests

the team at an inert training minefield at Binghamton University in Binghamton, New York State, as seen in Fig. 9a; in an area known to be relatively magnetically stable with minimal infrastructure. The field was seeded with inert TM-62M and TM-62P anti tank mines, with the TM-62 mines serving the role of a high-metal mine and the plastic-body TM-62P serving as an example of a low-metallic mine. The inert mines were set up in a checkered pattern at 6 m horizontal distances from one another and placed at depths of 5, 10, and 15, and 20 cm below the surface. The MFAM was moved along the surface at approximately 1 m/s along east-west survey lines. Then following integration with the robot, see Fig. 9b, the system was programmed to survey the 20 x 10 m site with 1m transects, meaning the robot traveled along ten 20 m long parallel lines spaced at 1 m.

Raw magnetic datasets were parsed and attributed with proper global navigation satellite systems (GNSS) time stamps using the NMEA string. Data were subsequently processed and cut to remove survey attributes. As these are total magnetic field data there were few artifacts associated with data acquisition; the data contained no dropouts, no spikes, and heading errors were not significant with respect to the high amplitude of the TM-62M

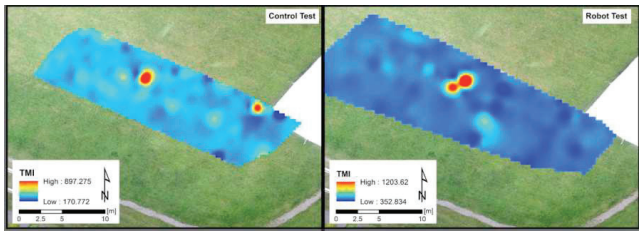

Fig. 10. Magnetic surveys using non-magnetic materials (left) and robot (right). Two inert TM-62M mines are clearly visible in the control test as high amplitude magnetic anomalies.

magnetic anomalies and as such required no heading or lag corrections over our test site. Although there was minimal impact on the results of this pilot study, directional heading errors could have a greater impact over larger survey areas, which may require additional data processing using line leveling algorithms (de Smet et al. (2021)). These pilot surveys were conducted in less than 10 minutes and thus we did not use a base station magnetometer to diurnally correct these data; however, longer surveys over larger areas will require a base station to correct for geomatic diurnal variation. The regional magnetic field values were calculated with the International Geomagnetic Reference Field and their values were removed to calculate the residual total magnetic intensity (TMI) in nanoTeslas (nT). These data were then exported as vector files, interpolated using kriging interpolation and re-generated as raster maps of TMI magnetic anomalies. The base map used in Figure 6 was collected with a DJI Phantom 4 Pro at 50 m above ground level (AGL) and were processed with Pix4Dmapper photogrammetry software to produce a GeoTIFF orthoimage file.

Weak linear north-south and east-west features can be seen in these data and are buried infrastructure that has been confirmed by ground-penetrating radar surveys (Figure 6). Two TM-62M antitank mines can be seen as red high amplitude features in the controlled test and as expected the plastic TM-62P mines were not able to be detected with magnetometry. Unfortunately the robotic test was slightly further south of the controlled test and was unable to resolve the second eastern TM-62M; however, the test results are fairly similar and show that the magnetic noise created by the robot motors is not great enough to compromise the validity of the magnetic surveys. Future research would investigate alternate post-processing methods to improve the visibility of inert mines, including destriping algorithms and reduction to the pole.

7. CONCLUSIONS

In this paper, the design, modeling, and implementation of an omnidirectional screw-driven robotic platform capable of operation in a broad range of terrains were presented. The robot was applied to a simulated humanitarian demining application. Based on the results of this work, the developed platform shows promise in field applications.

ACKNOWLEDGMENT

This work was supported by the National Science Foundation through OISE-1658696.

REFERENCES

Chan, S. (2013). Munitions risk education in cambodia. *The Journal of ERW and Mine Action*, 17.

de Smet, T.S., Nikulin, A., Romanzo, N., Graber, N., Dietrich, C., and Puliaiev, A. (2021). Successful application of drone-based aeromagnetic surveys to locate legacy oil and gas wells in Cattaraugus county, New York. *Journal of Applied Geophysics*, 186, 104250. doi: 10.1016/J.JAPPGEO.2020.104250.

DeAngelo, D. (2018). Demilitarizing disarmament with mine detection rats. *Culture and Organization*, 24(4), 285–302. doi:10.1080/14759551.2018.1488848.

Fracchia, M., Benson, M., Kennedy, C., Convery, J., Poultney, A., Anderson, J.W., Tan, A., Wright, J., Ermilio, J., and Clayton, G.M. (2015). Low-cost explosive ordnance disposal robot for deployment in southeast asia. *2015 IEEE Canada International Humanitarian Technology Conference, IHTC 2015*. doi: 10.1109/IHTC.2015.7238055.

Freeberg, J.T. (2010). *A Study of Omnidirectional Quad-Screw-Drive Configurations for All-Terrain Locomotion*. Ph.D. thesis, University of South Florida.

Fukushima, E.F., Freese, M., Matsuzawa, T., Aibara, T., and Hirose, S. (2008). Humanitarian demining robot gryphon–current status and an objective evaluation. *Internat. Journal on Smart Sensing and Int. Systems*.

He, D. and Long, L. (2018). Design and analysis of a novel multifunctional screw-propelled vehicle. *Proceedings of 2017 IEEE International Conference on Unmanned Systems, ICUS 2017*, 2018-January, 324–330. doi:10.1109/ICUS.2017.8278363.

Nagaoka, K., Kubota, T., Otsuki, M., and Tanaka, S. (2009). Development of Lunar Exploration Rover Using Screw Propulsion Units -Note on Dynamic Behavior and Moving Direction Control. *19th Workshop on JAXA Astrodyn. Flight Mech., Kanagawa, Japan*, 143–148.

Neumeyer, M.J. and Jones, B.D. (1965). The Marsh Screw Amphibian. *Journal of Terramechanics*, 2(4), 83–88.

Nikulin, A., de Smet, T.P., Puliaiev, A., Zhurakhov, V., Fasullo, S., Chen, G., Spiegel, I., and Cappuccio, K. (2020). Automated UAS Aeromagnetic Surveys to Detect MBRL Unexploded Ordnance. *The Journal of Conventional Weapons Destruction*, 24(1).

Nikulin, A. and de Smet, T.S. (2019). A UAV-based magnetic survey method to detect and identify orphaned oil and gas wells. *The Leading Edge*, 38(6), 447–452.

Open Development Cambodia (2020). SDG 18 Cambodia mine/ERW free - Open Cambodia (ODC). URL: https://opendevelopmentcambodia.net/topics/sdg-18-cambodia-

Osiński, D. and Szykiedans, K. (2015). Small remotely operated screw-propelled vehicle. *Advances in Intelligent Systems and Computing*, 351, 191–200. doi:10.1007/978-3-319-15847-119.

Safar, M.J., Chandradekaran, Y., Basah, S.N., Basaruddin, K.S., and Hashim, M.S. (2018). Kinematic analysis of a screw wheeled omnidirectional mobile robot. *Journal of Telecommunication, Electronic and Computer Engineering*, 10(1-15), 111–115.

Taheri, H., Qiao, B., and Ghaeminezhad, N. (2015). Kinematic Model of a Four Mecanum Wheeled Mobile Robot. *International Journal of Computer Applications*, 113(3), 6–9. doi:10.5120/19804-1586.